RESEARCH ARTICLE

NANO · MICRO small
www.small-journal.com

Mechano-Driven Neuromimetic Logic Gates Established by Geometrically Asymmetric Hydrogel Iontronics

*Yaowen Ouyang, Xiang Li, Yan Du, Yuyang Zhang, Zhong Lin Wang, and Di Wei**

The human brain's neural network demonstrates exceptional efficiency in information processing and recognition, driving advancements in neuromimetic devices that emulate neuronal functions such as signal integration and parallel transmission. A key challenge remains in replicating these functions while minimizing energy consumption. Here, inspired by neuronal signal integration and axonal bidirectional transmission, mechano-driven hydrogel logic gates leveraging the piezoionic effect is presented, offering a novel bionic approach with significantly reduced power consumption. By exerting external force on the thick and thin sides of the geometrically asymmetric hydrogel, spike signals of differing amplitudes and opposite polarities can be generated, corresponding to '1' and '0', respectively. The differential mobility of anions and cations plays a crucial role in the piezoionic effect. This geometric asymmetry amplifies ion convection, improving force-to-electricity conversion efficiency, while the inclusion of salts with varying ion size can further enhance this disparity, even reversing the signal direction. Arranging asymmetric hydrogel iontronics in series-parallel configurations enables the emulation of complex neuronal logic operations, facilitating ionic spike signal addition and subtraction. This hydrogel-based logic control has been directly applied in human-machine interaction to control robot arms and offers significant potential for the advancement of artificial intelligence, robotics, and wearable technologies.

1. Introduction

The Von-Neumann architecture, with its inherent limitations such as substantial energy consumption, heat dissipation, and temporal inefficiencies due to the separation of storage and processing, is encountering the boundaries of its potential.[1] As a result, a paradigm shift toward neural information processing, mimicking the natural mechanisms of living organisms, is emerging. This transition is pivotal for enhancing the capabilities of intelligence, which aims to replicate biological perception and signal processing. Inspired by the human brain, neuromorphic computing leverages highly integrated synapses to execute complex tasks with significantly lower energy consumption than traditional transistor-based circuits.[2] The brain uses analog computation to integrate the information inside the neuron, and the communication between the neurons is processed by the spike signal generated by the ions, which is fundamentally different from the present computer based on digital electronic circuits.[3] The integration of information processing in brain-like logic computing is pivotal for advancing artificial ionic skin perception and neural interface technologies, making the construction of iontronic-based neural logic computing a crucial challenge.[4] Hydrogels are particularly well-suited for bionic ion-regulated devices, combining solid-like morphology with efficient ionic conductivity, exceptional biocompatibility, and mechanical properties akin to human skin, thereby facilitating the advancement of neuromimetic systems.[5] Applications span from solid electrolytes in electrical double layer transistors[6] to nanofluid memristors.[7]

Y. Ouyang, X. Li, Y. Du, Z. L. Wang, D. Wei
Beijing Institute of Nanoenergy and Nanosystems
Chinese Academy of Sciences
Beijing 101400, P. R. China
E-mail: dw344@cam.ac.uk

Y. Ouyang, X. Li, Y. Du
School of Nanoscience and Engineering
University of Chinese Academy of Sciences
Beijing 100049, P. R. China

Y. Zhang
Department of Material Science and Engineering
The University of Manchester
Manchester M13 9PL, UK

Z. L. Wang
Beijing Key Laboratory of Micro-Nano Energy and Sensor
Center for High-Entropy Energy and Systems
Beijing Institute of Nanoenergy and Nanosystems
Chinese Academy of Sciences
Beijing 101400, P. R. China

Z. L. Wang
Georgia Institute of Technology
Atlanta, GA 30332-0245, USA

D. Wei
Centre for Photonic Devices and Sensors
University of Cambridge
9 JJ Thomson Avenue, Cambridge CB3 0FA, UK

The ORCID identification number(s) for the author(s) of this article can be found under https://doi.org/10.1002/smll.202409998

DOI: 10.1002/smll.202409998

Moreover, asymmetric trimer hydrogels can emulate synaptic plasticity when subjected to external pulsed electric fields.[8] Although underexplored, mechano-driven hydrogel neuromimetic devices hold significant potential for self-powered logic control, eliminating the need for an external power supply to operate the logic, thereby enhancing energy efficiency. Preliminary research indicates significant opportunities, particularly through the development of geometrically asymmetric hydrogel logic gates.

The piezoionic effect in hydrogels refers to the ion convection process within the hydrogel driven by a pressure gradient, facilitating ion migration and enabling signal transduction under mechanical stimulation.[9] The generation of the ionic signal is attributed to the differential mobilities of anions and cations within the hydrogel, where this disparity in movement under external stimulation leads to the formation of an electric potential.[9] By harnessing mechanical energy and converting it into electrical energy, piezoionic hydrogels can generate ionic currents, making them highly suitable for applications in self-powered artificial pressure sensors, iontronic skin, and biomedical sensors.[10] Compared to traditional ionic piezocapacitive sensors,[11] this mechanism offers a self-powered alternative for the development of advanced sensing technologies. Recent studies have primarily concentrated on enhancing the piezoionic coefficient to improve output performance by altering electrolyte salt content, cross-linking agents,[9] modifying polymer networks,[12] and doping with ionic plastic crystals etc.[13] Enhancing the piezoionic coefficient of hydrogel iontronics while amplifying the diffusion rate disparity between anions and cations remains a critical challenge. Furthermore, the nonlinear piezoionic response of hydrogels to applied pressure has shown potential as a threshold gating mechanism, offering promising information processing capabilities that could serve as alternatives to traditional transistors in logical gate.[14] Nevertheless, the potential of hydrogel iontronics for biomimetic neural networks in logic computation remains largely untapped. Specifically, the development of mechano-driven hydrogel ionic logic gates, which promise self-powered neuromimetic systems, represents a significant opportunity for future breakthroughs.

In neural transmission, the release of neurotransmitters is controlled by the synaptic front end, which makes the electrical signal transmission on neurons unidirectional, but the action potential caused by Na^+ and K^+ reflux on the axon can be transmitted in both directions, depending on the location of the stimulation. This is miraculously similar to the piezoionic effect, that is, when an external force is applied to different sides of the same hydrogel, it will cause ion convection in the opposite direction, which is very suitable as the '1' and '0' input signals of the logic gate. In order to further amplify the recognition of '1' and '0' spike signals, we prepared hydrogels with asymmetric thickness on both sides. Due to the different pressures applied by the motor on different sides at the same step length, two kinds of ionic spike signals with different amplitudes and directions will be generated when pressing the geometrically asymmetric hydrogel. The regulation of mobility differences between anions and cations is critical for the piezoionic effect. This geometric asymmetry circumvents the need for complex chemical synthesis and molecular design, thereby enhancing signal recognition and accelerating ion convection velocity. Additionally, it improves force-to-electricity conversion efficiency. The incorporation of salts with varying ion sizes can further amplify this disparity and even reverse the direction of the electrical signal. It should also be noticed that the brain is interconnected through synapses in the neuronal network, and the processing of information is a process of dynamically integrating spike signals. Inspired by this, we used a simple series-parallel circuit of multiple geometric asymmetric hydrogels to simulate the integration process of spike signals between multiple neurons. Under the influence of an external force field, the amplitude and direction of input spike signals generated by various hydrogels are modulated, thereby emulating the weighting of output signals at the synaptic front end of neurons in a neural network. This process facilitates the logical addition and subtraction of spike signals, ultimately allowing for the regulation of the amplitude and direction of the output spike signal. Consequently, four types of mechano-driven hydrogel logic gates have been developed, broadening the scope for new logic gate applications. These logic gates are well-suited for human-machine interaction, functioning as self-powered systems that significantly reduce energy consumption in logic control. Moreover, through strategic design and patterning of thickness, hydrogel logic gates can be seamlessly integrated into robotic iontronic skins, offering a promising approach for human-machine interaction and paving the way for innovative self-powered logic circuits.

2. Results

2.1. Brain-Like Hydrogel Logic Gates

The human sense of touch originates from receptors in the skin. Synapses release neurotransmitters, which open ion channels. The reflux of sodium and potassium ions causes changes in nerve membrane potential and forms action potentials. The signals are transmitted along nerve axons to the brain, which recognizes the signals and ultimately gives instructions to the human body. Inspired by the transmission of electrical signals along axons, mechano-driven hydrogel logic gates were developed for application in the logic control processes of human-machine interaction (**Figure 1a**). The operational principle of bionic hydrogel logic gates is derived from the piezoionic effect. By applying pressure to each side of the geometrically asymmetric hydrogel, the direction of ion convection is altered, generating current and voltage signals in opposing directions. This characteristic is ideally suited for encoding '1' and '0' electrical signals, forming the foundation for the functionality of logic gates.

Inspired by the neural network to control the output signal by modulating the weight of the input ionic spike signal of multiple synaptic front ends, four logic gates were constructed using a straightforward series-parallel configuration of asymmetric hydrogels, as illustrated in Figure 1b. By strategically assigning signal generation weights to different hydrogels, the integration of signals among multiple neurons is simulated, enabling the realization of electrical signal outputs under various logical input states.

2.2. Performance of Asymmetric Hydrogel Iontronics

To enhance the differentiation and recognition of the input signal, the hydrogel is constructed in an asymmetric configuration

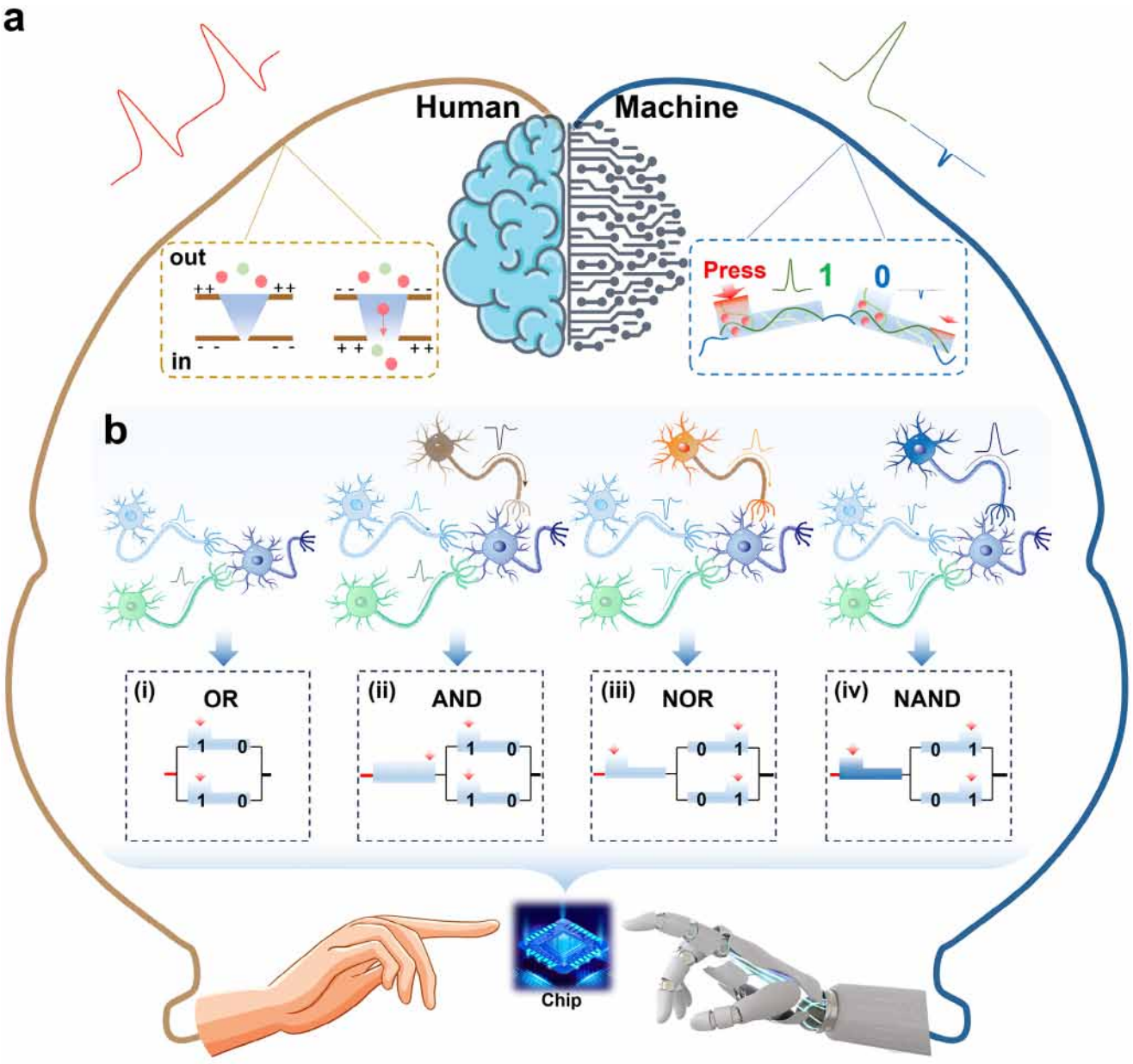

Figure 1. Conceptual description of mechano-driven neuromimetic logic gates. a) Mechano-driven hydrogel iontronics for logic control of human-machine interaction. b) Inspired by the regulation of brain-like neuron network, four kinds of iontronic logic gates realized by simple series-parallel connections.

with varying thicknesses on each side, while the motor's step size is fixed to regulate pressure. Due to the varying pressures exerted by the motor on each side at the same step length, the geometrically asymmetric hydrogel generates two types of ionic spike signals with distinct amplitudes and directions. The thicker side, subjected to greater pressure, produces a higher amplitude electrical signal, while the thinner side yields a lower amplitude.

The length, width and height of the symmetrical hydrogel are 30, 10, and 2 mm, respectively. The asymmetric hydrogel, with a 1 mm height differential, was fabricated using a custom acrylic mold and UV initiation (Figure S1, Supporting Information). The prepared hydrogel was positioned on an acrylic plate with a copper wire electrode secured using double-sided adhesive (with an electrode separation of 20 mm). The hydrogel was then covered with PET tape for encapsulation and stabilization, minimizing any interference during hydrogel extrusion (Figure S2, Supporting Information). To identify the influence of geometry structure change on device output, open-circuit voltage (V_{oc}) and short-circuit current (I_{sc}) of asymmetric hydrogel under different pressures were tested, and symmetric hydrogel was set as the control group. The pressure was applied to the asymmetric hydrogel thick side through the indenter (10 mm × 10 mm) fixed on the motor and controlled by the forward distance of the motor (**Figure** 2a). A thin-film pressure sensor is set below the

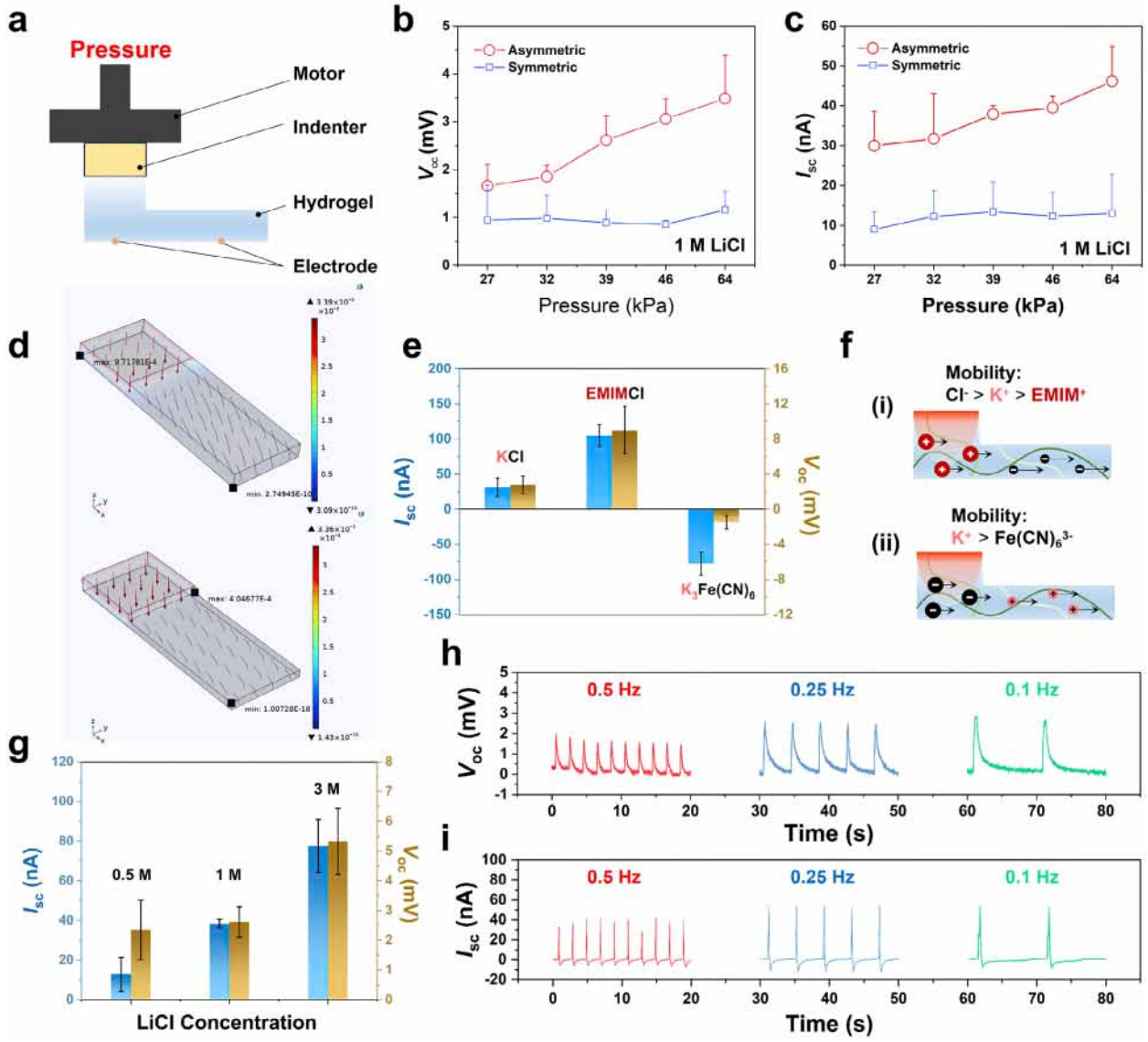

Figure 2. Performance characterization of asymmetric hydrogel iontronics. a) Schematic diagram of hydrogel performance test method. b) V_{oc} comparison of symmetric and asymmetric PAAm hydrogels under different pressures, containing 1 M LiCl at a frequency of 0.5 Hz (data are mean ± SD, N = 3). c) I_{sc} comparison of symmetric and asymmetric PAAm hydrogels under different pressures, containing 1 M LiCl at a frequency of 0.5 Hz (data are mean ± SD, N = 3). d) COMSOL simulation of fluid velocity of symmetric and asymmetric hydrogels. e) V_{oc} and I_{sc} of asymmetric PAAm hydrogels with different ionic salt (C = 1 M) under the pressure of 39 kPa, with the frequency of 0.5 Hz (data are mean ± SD, N = 3). f) Schematic diagram of the difference in ion mobility rate caused by the difference in anion and cation radius. g) The V_{oc} and I_{sc} of asymmetric PAAm hydrogel with different LiCl concentration under the pressure of 39 kPa, with the frequency of 0.5 Hz (data are mean ± SD, N = 3). h,i) are respectively V_{oc} and I_{sc} of asymmetric PAAm hydrogel with 1 M LiCl at different frequencies under the pressure of 39 kPa.

hydrogel to measure the pressure under the static distance of the motor (Figure S3a, Supporting Information), and the relationship between pressure and the step distance of the motor is described by the fitting function: P (kPa) = 37.3 × Distance (mm) + 8.87, R^2 = 0.96448 (Figure S3b, Supporting Information). Within the pressure range tested in the experiment, V_{oc} and I_{sc} of the two structures of hydrogel devices increased with the lifting of pressure, the curve growth rate of asymmetric hydrogel was larger, and the overall curve was above the symmetric hydrogel (Figure 2b,c), which showed that asymmetric hydrogel had higher force-electricity conversion efficiency than symmetric hydrogel under the same conditions. The resistance of symmetric and asymmetric PAAm hydrogels, containing 1 M LiCl, was assessed via electrochemical impedance spectroscopy (EIS). The resistance values, determined from the intersection of the Nyquist plot with the real axis, were ≈270 Ω for the symmetric hydrogel and 520 Ω for the asymmetric hydrogel (Figure S4, Supporting Information). This might be attributed to the smaller volume of the asymmetric hydrogel with less total number of ions. At a pressure of 27 kPa, the V_{oc} of the asymmetric hydrogel was ≈1.75 mV, compared to 1.5 mV for the symmetric hydrogel with $\triangle V_{(27kPa)}$ of 0.25 mV. As the pressure increased to

64kPa, the V_{oc} of the asymmetric hydrogel reached ≈3.5 mV, while the symmetric hydrogel remained at ≈1.5 mV, resulting in a $\triangle V_{(64kPa)}$ of 2 mV. The I_{sc} of asymmetric and symmetric hydrogel also showed a similar trend. The V_{oc} and I_{sc} signal waveforms of symmetric and asymmetric hydrogels at different pressures could be seen in Figures S5 and S6 (Supporting Information), respectively. The enhanced output performance of asymmetric hydrogels can be attributed to the increased stress concentration at the plateau induced by the discontinuity in the hydrogel matrix, which amplifies ion convection. Conversely, the continuous matrix of the symmetric hydrogel leads to stress dissipation beyond the pressure application zone. To substantiate this hypothesis, finite element analysis was employed to simulate stress and strain distributions in both symmetric and asymmetric hydrogels under static pressure. The stress distribution states of two kinds of hydrogels were shown in Figure S7 (Supporting Information), under the same pressure of 10 kPa and same area (10 mm × 10 mm). The stress of symmetric hydrogel was distributed in a "U" shape, and the opening was toward the area without pressure application, with a range of ≈3.58–7.16 kPa from theoretical modeling. On the contrary, due to the existence of a plateau, the stress distribution of the asymmetric hydrogel was "O" shaped. The color of the stress distribution map at the plateau was relatively bright, ≈7.12–14.2 kPa, indicating that the stress was relatively concentrated. The distribution map of strain also showed a similar distribution. As the pressure increased, the stress and strain gradually increased (Figures S8 and S9, Supporting Information). The stress and strain changes of the asymmetric hydrogel at the plateau were greater than those of the symmetric hydrogel, indicating that the stress was further concentrated, which could explain why the V_{oc} and I_{sc} of the asymmetric hydrogel change more with the increase in pressure. In addition, the fluid flow in symmetric and asymmetric hydrogel under the action of force field was simulated by COMSOL MultiPhysics 6.2 software (Figure 2d). Under the pressure of 10 kPa, the average Darcy velocities of symmetric and asymmetric hydrogel were 1.255×10^{-4} and 1.638×10^{-4} m s^{-1}, respectively. This result showed that the asymmetric shape successfully increased the flow rate of water in the hydrogel.

The difference in the mobility rate of anions and cations in hydrogels was considered to be a necessary condition for the occurrence of ionic currents in hydrogels induced by stress gradients. Assuming that the mobility rate of anions and cations with the solvent was completely consistent, the net current of anions and cations was zero, which obviously did not match the experimental facts. The difference in the movement rate of anions and cations in hydrogels can be explained by the selectivity of 3D network pores in hydrogels to different ions.[9] Theoretically, ions with small sizes are easier to pass through these pores than larger ions. The speed of ions in the hydrogel can be given by the following formula:[9]

$$v_+ = \frac{D_+}{D_{0+}}v, \quad v_- = \frac{D_-}{D_{0-}}v \tag{1}$$

where, v_+, v_-, and v respectively represent the movement speed of cations, anions, and solvent in the hydrogel, D_{0+} and D_{0-} are the diffusion coefficients of cations caused by solution, and D_+ and D_- are the measured diffusion coefficients of cations and anions in the hydrogel. The relationship between voltage and the difference of ion speed in the hydrogel can be given by the following formula:[9]

$$\nabla V = \alpha \nabla P \tag{2}$$

$$\alpha = -\frac{eN\kappa}{\sigma\eta}\left[\frac{D_+}{D_{0+}} - \frac{D_-}{D_{0-}}\right] \tag{3}$$

where, α is the piezoionic coefficient, e is the electronic charge, N is the concentration, κ is the matrix permeability, σ is the conductivity and η is the fluid viscosity. Based on the above theory, the piezoionic coefficient can be increased by selecting the ionic salt with a large difference in the size of the anion and cation, and the voltage output can be improved at the same pressure gradient. In addition, the direction of the ionic current can also be changed. To verify the influence of different ion size, hydrogels containing three different types of salts were compared, and the experimental results were shown in Figure 2e. As a contrast, KCl was a salt with relatively small difference between the size of anions and cations. The diameters of K^+ and Cl^- were ≈0.266 and 0.167 nm,[12a,15] respectively, and their I_{sc} and V_{oc} were 31 nA and 2.7 mV, respectively. This was similar to the signal amplitude of PAAm hydrogel with LiCl under the same conditions (38 nA and 2.6 mV, respectively). 1-Ethyl-3-methylimidazolium chloride (EMIMCl) was chosen as a representative for the larger cations, given that the sizes of $EMIM^+$ exceed that of Cl^-, a distinction that is consistent with the molecular structure. The I_{sc} and V_{oc} of the corresponding hydrogel iontronics were ≈105 nA and 9 mV, respectively, which are significantly higher than KCl. In addition, potassium ferricyanide [$K_3Fe(CN)_6$] was chosen as the research object for larger anions, and the diameters of $Fe(CN)_6^{3-}$ was ≈0.45 nm.[12a,16] Despite the disparity in valence between $Fe(CN)_6^{3-}$ and Cl^-, the PAAm hydrogel, as a neutral polymer, allows the coulomb force between the ions and the polymer chains to be effectively disregarded. The direction of I_{sc} and V_{oc} of PAAm hydrogel containing $K_3Fe(CN)_6$ was opposite to that of KCl and EMIMCl, with amplitudes of -78 nA and −1.5 mV, respectively. The voltage and current signal waveforms of hydrogels containing these three kinds of salts were shown in Figure S10 (Supporting Information). The reversal of current and voltage signal directions could be attributed to the size of $Fe(CN)_6^{3-}$ being greater than K^+. For EMIMCl, the size of Cl^- is smaller than that of $EMIM^+$, so the mobility of the former was much faster than latter. When the stress gradient was applied to one side of the hydrogel, Cl^- rapidly moved from the deformation area to the non-deformation, and $EMIM^+$ was left behind [Figure 2f (i)]. When the salt in the hydrogel was replaced by $K_3Fe(CN)_6$, K^+ rapidly moved from the deformation to the non-deformation area, at this time, the larger $Fe(CN)_6^{3-}$ were left behind, so the ion flux switched [Figure 2f (ii)]. The smaller voltage amplitude might be due to the PAAm hydrogel containing $K_3Fe(CN)_6$ prepared by different methods. The swelling process made the network pores of the 3D polymer chain larger, so the selectivity to $Fe(CN)_6^{3-}$ decreased. The corresponding resistance of three kinds of salt-containing ionic hydrogels were measured to be ≈100, 300, and 560 Ω by EIS, corresponding to $K_3Fe(CN)_6$, KCl and EMIMCl, respectively (Figure S11, Supporting Information). Although the V_{oc} of PAAm hydrogel containing $K_3Fe(CN)_6$ was less

than KCl, and the smaller internal resistance might be the reason why its I_{sc} (78 nA) was greater than KCl (31 nA). The influence of salt concentration on electrical output was shown in Figure 2g. With the increase in LiCl concentration from 0.5 to 1 and 3 M, I_{sc} increased from 13 to 38 and 77 nA, and V_{oc} increased from 2.3 to 2.6 and 5.3 mV, respectively. The signal waveforms of voltage and current at different concentrations can be seen in Figure S12 (Supporting Information). The result showed that the electric output of the hydrogel iontronics increased monotonously with the increase of ionic salt concentration (from 0.5 to 1 and 3 M), which could be attributed to the existence of more ions in the hydrogel. The EIS of hydrogels with different ion concentrations was carried out. With the increase of ion concentration (from 0.5 to 1 and 3 M), the corresponding ion resistance decreased significantly, which was ≈1.1, 0.5, and 0.18 kΩ, respectively (Figure S13, Supporting Information). The effect of different force frequency on the performance of asymmetric PAAm hydrogel iontronics containing LiCl was also studied. As the frequency gradually decreased (from 0.5 to 0.25 and 0.1 Hz), the peak of V_{oc} and I_{sc} have larger amplitudes. The V_{oc} increased from 2 to ≈2.5 and 2.9 mV (Figure 2h), while the I_{sc} increased from 40 to ≈55 nA (Figure 2i). This may be attributed to the relaxation of ion transport, whereby ion movement requires a finite duration rather than occurring instantaneously. When the pressure is applied on the hydrogel, the stress gradient would induce ion convection. This process inevitably led to the imbalance of the spatial distribution of anions and cations in the hydrogel, resulting in the formation of local ion concentration difference. The re-equilibrium of concentration diffusion required a certain amount of time. Once the force stops, the concentration balances, and the signal amplitude is restored to some extent upon reapplication of the force. This was obvious for the frequency experiment of hydrogels containing EMIMCl, and the peak of voltage and current were attenuated (Figure S14, Supporting Information). Once the force stops for a period of time, the concentration balances, and the signal amplitude is restored to some extent upon reapplication of the force (Figure S15, Supporting Information). Interestingly, during the continuous external force experiment of hydrogel iontronics containing EMIMCl, it was observed that the positive ionic current amplitude continued to decrease, while the negative ionic current amplitude increased, and the current waveform basically reversed after ≈700 cycles (Figure S16, Supporting Information). This phenomenon could also be attributed to the effect of completely depressing ion convection after the accumulation of ion concentration difference reaches a certain extent. This signal form of ionic spike signal decaying with time can be used to simulate the memory forgetting process of depression. When the frequency of the applied pressure is fixed and the amplitude of pressure is increased at the same time, the ionic spike signal continues to increase with time. This signal form can be used to simulate the memory enhancement process of neural excitation.

2.3. Logic Gates Constructed by Asymmetric Hydrogel Iontronics

The inherent separation of storage and computation in the Von-Neumann architecture leads to prolonged data retrieval, elevated energy consumption, and excessive heat dissipation. These limitations have catalyzed the development of neuromimetic devices.[17] Despite lacking the immense computational power of computers, the human nervous system excels in perception and computation with significantly lower energy consumption and heat generation.[18] Unlike robots that use digital signals as encoding for information, information transmission in living organisms uses analog spike signals generated during life activities.[19] Therefore, the processing of analog signals is the foundation for the implementation of neural device perception and logical computation. Subsequently, four types of hydrogel logic gates are demonstrated under the influence of a force field. Through the series-parallel configuration of hydrogel iontronics, logical operations such as addition and subtraction of spike signals are achieved.

The fundamental requirement for logic gates is the presence of two distinct signal states, representing high and low amplitudes. In this study, signals were generated by applying pressure to both sides of the hydrogel. By controlling the motor's displacement, the thicker side of the hydrogel experienced greater pressure, while the thinner side experienced less, resulting in electrical signals with varying amplitudes. In addition, the force acting on different sides of the hydrogel will cause the opposite ion convection process (the diagram can be seen in Figure S17, Supporting Information). The formation of the opposite direction of the electrical signal process will not only improve signal recognition but imitate the excitation and inhibition process of the neuron signal input. The input signals generated when pressuring the thick and thin sides of the asymmetric hydrogel were defined as input ″1′ and '0', respectively (**Figure 3a**). At the same time, a threshold was defined (45 nA), and the output of the current amplitude exceeding the threshold was defined as '1', otherwise '0'. The truth table of the four logic gates was shown in Figure 3b. Here, the current spike signal was chosen to demonstrate the working of these four hydrogel logic gates, and the corresponding voltage signal can be viewed in Figure S18 (Supporting Information). OR gate was the most basic one, achieved by connecting two asymmetric hydrogels in parallel (Figure 3c). For the convenience of description, the two hydrogels were noted as A and B respectively. Since '1+0' and '0+1' are fundamentally equivalent, the waveforms are merged. The corresponding current signal was shown in Figure 3g. If A = B = 1, the peak current superposition was the largest, which obviously exceeded the threshold (set 45 nA), so the output was '1'. When A = 1 and B = 0 (A = 0 and B = 1), the net peak current amplitude was still higher than the threshold, and '1' was still output. However, if A = B = 0, the current amplitude was about −30 nA, significantly lower than the threshold, the output was '0'. More specific operating mechanism was showed in Figure S19 (Supporting Information). In addition, the AND gate was built on the basis of OR gate. Another hydrogel was introduced in series in the circuit module of two parallel hydrogels, marked as S, which was set as a signal source that continuously emitted negative currents (Figure 3d). The corresponding current signal was shown in Figure 3h. If A = B = 1, the amplitude of net peak current was greater than the threshold, and the output was '1'. Once A = 1 and B = 0 (A = 0 and B = 1), the amplitude of net current was less than the threshold current and the output was '0'. Obviously, when A = B = 0, the current signal was in the same direction as the S, less than the threshold, and the output is '0'. Figure S20 (Supporting

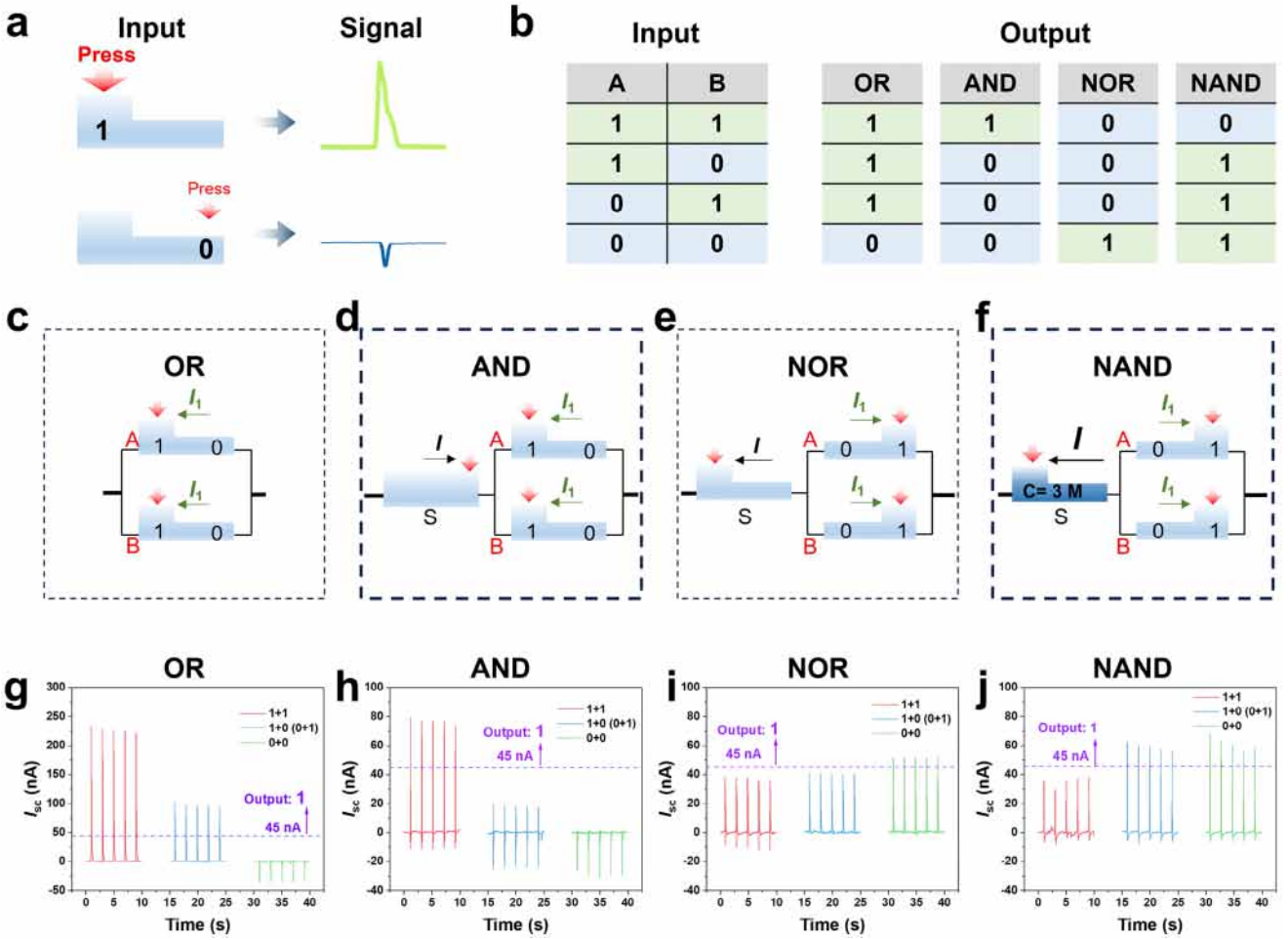

Figure 3. Mechano-driven hydrogel logic gates. a) Define input: apply pressure on the thick and thin sides of the asymmetric hydrogel as input '1' and '0' respectively. b) Truth table of four types of hydrogel logic gates. c–f) referred to the structure of OR, AND, NOR, and NAND logic gates, respectively. g–j) referred to I_{sc} of four hydrogel logic gates under different logic addition and subtraction. Define output: set the threshold to 45 nA, the peak current amplitude exceeding the threshold defined as output '1', otherwise '0'.

Information) shows the operating mechanism. NOR gate was based on the idea of AND gate. The difference was that the hydrogel S produced a positive spike current signal. At this time, due to the change of the structural direction of hydrogels A and B in the circuit, a negative peak current signal was generated when '1' was input, and a positive peak current signal was generated when '0' was input (Figure 3e). The corresponding current signal can be seen in Figure 3i. If A = B = 1, together with A = 1 and B = 0 (A = 0 and B = 1), the output current amplitude was less than the threshold, so the output was '0'. Only when A = B = 0, the net current was greater than the threshold, the output was '1'. The specific operating mechanism could be seen in Figure S21 (Supporting Information). In NAND gate, the hydrogel with LiCl concentration of 3 M was selected as the continuous positive pulse current signal source. At this time, the current signal of input '1' of hydrogel A and B was a negative spike signal, and the current signal of input '0' was positive (Figure 3f). The current signal was shown in Figure 3j. If A = B = 1, the net current amplitude was less than the threshold, and the output was '0'. When A = 1 and B = 0 (A = 0 and B = 1), the peak current was higher than the threshold and the output was '1'. If A = B = 0, the amplitude of the peak current signal reached the maximum, and the output was obviously '1'. A more specific operating mechanism was demonstrated in Figure S22 (Supporting Information).

2.4. Mechano-Driven Neuromimetic Logic Gates for Human-Machine Interaction

Leveraging its pressure sensing and signal processing capabilities, the mechano-driven neuromimetic logic gates based on hydrogels can facilitate human-machine interactions, specifically in robotic logic control. As proof of concept, OR and AND gates were demonstrated. Analogous to the neural network"s signal recognition and integration process, the OR gate can be seen as a mechanism where two input neurons, A and B, generate excitatory signals that are integrated by the output neuron (**Figure 4a**). The AND gate consists of three neurons A, B, and S, where A and B as input neurons release excitatory signals to the output neuron, while S continuously outputs inhibitory signals (Figure 4b).

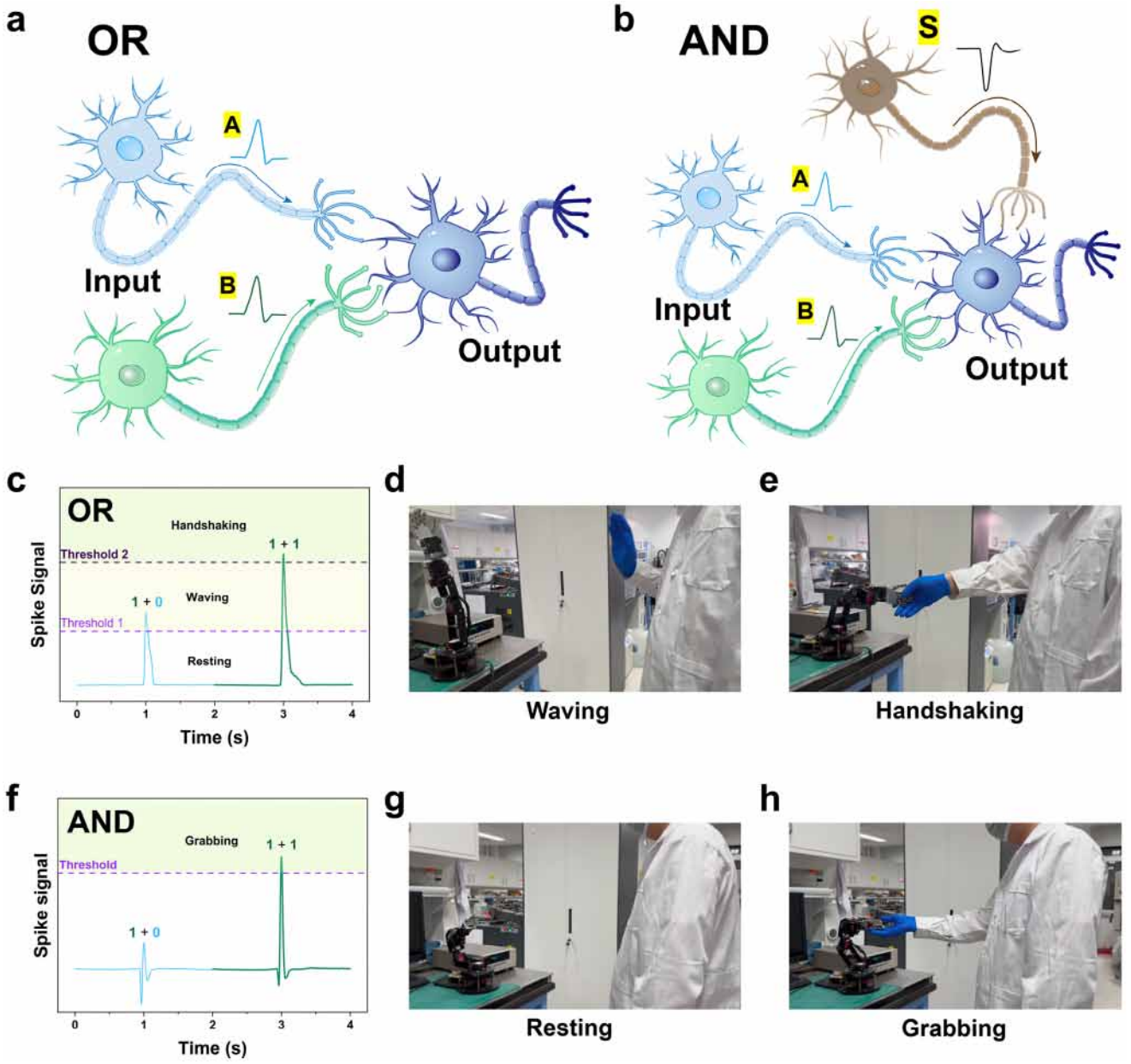

Figure 4. Mechano-driven neuromimetic logic gates for human-machine interaction. a) The neural network diagram of OR gate, neurons A and B release excitatory signals. b) Neuron network diagram of AND gate. Neuron S releases inhibitory signals, while neurons A and B release excitatory signals. c) Schematic diagram of threshold setting for OR gate. d) Waving action of the robotic arm was triggered when the signal amplitude exceeded threshold 1. e) Handshaking action of the robotic arm was triggered when the signal amplitude exceeded threshold 2. f) Schematic diagram of threshold setting for AND gate. g) The rest state of the robotic arm. h) Grasping action of the robotic arm was triggered once the signal amplitude exceeded the threshold.

At this time, the excitation signal of any one of A and B will be weakened by S, and only A and B can release the excitation signal at the same time to exceed the set threshold.

The electrical signals generated by the hydrogel logic gates were recorded using a 6514 electrometer, and the actions of the robotic arm were controlled via LabVIEW software, thus achieving the human-machine interaction. For OR gate, two thresholds were set to achieve two actions of the robotic arm (Figure 4c; Video S1, Supporting Information). If hydrogel A and B had only one input '1', the generated spike signal could only exceed the threshold value 1 and trigger the waving action (Figure 4d). Once both A and B input 1, the signal amplitude exceeds threshold 2, triggering the second handshake action, shown in Figure 4e. AND Gate was set a threshold value to trigger the grabbing action (Figure 4f; Video S2, Supporting Information). As the emission source of the continuous negative spike signal, the hydrogel S could not trigger the threshold, while the hydrogel A and B still could not trigger the threshold when there was and only one input '1', and the robotic arm maintained the initial static state (Figure 4g). Only when A and B input '1' at the same

time, the threshold was reached, and the grasping action was triggered (Figure 4h). Although the control panel for the hydrogel logic gate was separated from the robot in this demonstration, hydrogel is a versatile material for iontronic skin. With appropriate circuit design and patterning, it is anticipated that tactile perception and logic control can be seamlessly integrated into the skin. Moreover, combining multiple mechano-driven hydrogel logic gates could enable novel logic operations, reducing power consumption while achieving functions comparable to those of current digital circuit chips.

3. Conclusion

Geometrical asymmetry plays a pivotal role in tuning the physical properties of materials and enhancing device performance. For instance, rolling zero-bandgap graphene into carbon nanotubes introduces a bandgap, transforming its electronic characteristics. The introduction of geometric changes presents significant implications for the design of next-generation devices and electronics. Although hydrogels have been widely studied as a component material of neuromimetic devices, the self-powered brain-like intelligent hydrogel logic gates based on the force field seems to have not attracted much attention. Leveraging the piezoionic properties of hydrogels, this study applied force to a hydrogel with asymmetric thickness to generate ionic spike signals of varying amplitudes and opposite directions, representing binary logic inputs as '1' and '0'. This difference in geometric structure not only avoids complex chemical synthesis and molecular design, but also magnifies the recognition of the signal and enhances the ion convection process, which can be attributed to stress concentration caused by the discontinuity of the polymer matrix. Moreover, incorporating salts with varying ion sizes can further amplify the disparity in ion mobility, potentially reversing the direction of the electrical signal by tuning hydrogels with different salts [such as EMIMCl and $K_3Fe(CN)_6$]. In addition, the increase in the salt concentration and the decrease in the frequency of the pressure have an effect on the increase of the spike signal amplitude. The thickness-asymmetric hydrogel iontronics was configured as a simple series-parallel circuit to mimic the integration of ionic spike signals across multiple neurons. By modulating the amplitude and direction of the ionic signals generated by the hydrogel, the weight variation in neuronal signal processing was simulated, enabling the logical operation of mechano-driven ionic spike signals. As a conceptual verification, the mechano-driven hydrogel logic gates were successfully applied to the logic control process of human-machine interaction. Geometrical asymmetry presents a transformative paradigm for modulating piezoionic behavior, significantly enhancing ion transport and responsiveness to mechanical stimuli. This approach could optimize ionic charge distribution, paving the way for high-efficiency, self-powered systems applicable in soft robotics and energy harvesting. The development of a mechano-driven hydrogel logic gate with in situ pressure sensing enables brain-like computation with minimal energy consumption, facilitating the integration of tactile perception and logical control through precise thickness regulation. This strategy holds substantial promise for advancing artificial intelligence, robotics, and wearable technologies.

4. Experimental Section

Materials: Acrylamide (AAm, 99%), Methylene-Bis-Acrylamide (MBAA, 99%), 2-Hydroxy-4′-(2-hydroxyethoxy)-2-methylpropiophenone (2959), Lithium chloride (LiCl, 99%), potassium chloride (KCl, 99%), 1-Ethyl-3-methylimidazolium chloride (EMIMCl) and potassium fericyanide [$K_3Fe(CN)_6$, 99%] all purchased from Macklin and used as received.

Preparation of Hydrogel: AAm (750 mg, monomer), MBAA (7.5 mg, cross-linker), 2959 (50 mg, photo-initiator) were dissolved in D.I. water (5 mL). Lithium chloride (LiCl) was weighed according to the required concentration and dissolved in it. EMIMCl was added to the volumetric flask due to strong deliquescence, and then other reagents were added to prepare the hydrogel solution precursor. Then it was injected into the self-made acrylic mold and placed under ultraviolet light for 20–30 min. After curing, it was taken out for experiment. To be noted, PAAm hydrogels containing $K_3Fe(CN)_6$ were prepared by swelling. The PAAm hydrogel (salt-free) was prepared according to the above ratio and dehydrated in a thermostatic drying chamber at 60 °C until the mass did not change significantly. Then it was put into $K_3Fe(CN)_6$ aqueous solution (1 M) to swell to a volume close to the initial size (≈1 h).

Fabrication of Hydrogel Iontronics: The copper wire electrode was fixed on the acrylic board by double-sided adhesive, and the electrode surface was fully infiltrated with a small amount of deionized water. The hydrogel was located on it to ensure that no bubbles between the hydrogel and the electrode, so as to avoid the capacitance change of the electrode interface caused by insufficient contact. Finally, the hydrogel was encapsulated on the acrylic plate by using PET tape.

Characterization and Measurements: A step motor (Linear Motion 1100) was used to provide the input of mechanical motions. Signals were collected by a test system consisting of an electrometer (6514, Keithley, USA) and a data acquisition card (BNC-2120, National Instruments, USA). All electrochemical properties were carried out by electrochemical workstation (Multi Auto-lab M204). Electrochemical impedance spectroscopy (EIS) was measured in the range of 0.1 MHz to 1 Hz.

Finite Element Analysis: The average Darcy flow rate of solvent in geometrically symmetric and asymmetric hydrogels was simulated by Multi-Physics 6.2 software. The length, width and height of the symmetrical hydrogel are 30, 10, and 2 mm, respectively. The asymmetric hydrogel, with a 1 mm height differential. A pressure of 1 N was applied on the platform area (1 cm^2) of the asymmetric hydrogel. The modulus, Poisson's ratio, and porosity of the hydrogel were set to 10^5 Pa, 0.499, and 0.8, respectively. ANSYS 2020 software was used to simulate stress and strain distribution diagram of geometrically symmetric and asymmetric hydrogels when the applied pressure was 10, 30, and 50 kPa respectively. The size, modulus, and Poisson's ratio of the hydrogel were all set to the above values, and the density of the hydrogel was set to 3.25 g cm^{-3}.

Supporting Information

Supporting Information is available from the Wiley Online Library or from the author.

Acknowledgements

This work was supported by the National Natural Science Foundation (grant number 22479016).

Conflict of Interest

The authors declare no conflict of interest.

Author Contributions

D.W. and Z.L.W. proposed the idea and the project. D.W. supervised the whole project. Y.W.O.Y. designed all the experiments and carried out the

experiments in this paper and analyzed the corresponding data. X.L. assisted in experimental testing and completed the finite element theoretical analysis model. Y.D. helped to realize the application of human-machine interaction. Y.Y. Z. finished the theoretical modeling of COMSOL. All the authors discussed the results and commented on the manuscript. D.W. and Y.W.O.Y. wrote this paper.

Data Availability Statement

The data that support the findings of this study are available from the corresponding author upon reasonable request.

Keywords

human-machine interaction, hydrogel iontronics, mechano-driven logic gates, neuromimetic devices, piezoionic

Received: October 25, 2024
Revised: February 26, 2025
Published online: March 6, 2025

[1] a) H. Chun, T. D. Chung, *Annu. Rev. Anal. Chem.* **2015**, *8*, 441; b) D. G. Roe, D. H. Ho, Y. Y. Choi, Y. J. Choi, S. Kim, S. B. Jo, M. S. Kang, J.-H. Ahn, J. H. Cho, *Nat. Commun.* **2023**, *14*, 5; c) T. Wang, J. Meng, X. Zhou, Y. Liu, Z. He, Q. Han, Q. Li, J. Yu, Z. Li, Y. Liu, H. Zhu, Q. Sun, D. W. Zhang, P. Chen, H. Peng, L. Chen, *Nat. Commun.* **2022**, *13*, 7432.

[2] a) A. Chanthbouala, V. Garcia, R. O. Cherifi, K. Bouzehouane, S. Fusil, X. Moya, S. Xavier, H. Yamada, C. Deranlot, N. D. Mathur, M. Bibes, A. Barthelemy, J. Grollier, *Nat. Mater.* **2012**, *11*, 860; b) L. Chen, M. Ren, J. Zhou, X. Zhou, F. Liu, J. Di, P. Xue, C. Li, Q. Li, Y. Li, L. Wei, Q. Zhang, *Proc. Natl. Acad. Sci. USA* **2024**, *121*, 2407971121; c) D. Hassabis, D. Kumaran, C. Summerfield, M. Botvinick, *Neuron* **2017**, *95*, 245; d) S. Li, Z. Zhang, F. Yang, X. Li, P. Peng, Y. Du, Q. Zeng, M. Willatzen, Z. L. Wang, D. Wei, *Device* **2024**, *2*, 100332.

[3] a) D. Marković, A. Mizrahi, D. Querlioz, J. Grollier, *Nat. Rev. Phys.* **2020**, *2*, 499; b) W. Gerstner, W. M. Kistler, R. Naud, L. Paninski, *Neuronal Dynamics: from Single Neurons to Networks and Models of Cognition*, Cambridge University Press, Cambridge, UK **2014**; c) Y. Zhang, J. Pei, Z. Huang, L. Jiang, K. Yin, J. Jiang, *Adv. Funct. Mater.* **2024**, *34*, 2400822; d) J. Su, Y. Li, D. Xie, J. Jiang, *Mater. Horiz.* **2023**, *10*, 1745; e) Y. Li, K. Yin, Y. Diao, M. Fang, J. Yang, J. Zhang, H. Cao, X. Liu, J. Jiang, *Nanoscale* **2022**, *14*, 2316.

[4] a) J. Yu, Y. Wang, S. Qin, G. Gao, C. Xu, Z. Lin Wang, Q. Sun, *Mater. Today* **2022**, *60*, 158; b) S. Dai, X. Liu, Y. Liu, Y. Xu, J. Zhang, Y. Wu, P. Cheng, L. Xiong, J. Huang, *Adv. Mater.* **2023**, *35*, 2300329; c) X. Li, R. Li, S. Li, Z. L. Wang, D. Wei, *Nat. Commun.* **2024**, *15*, 6182; d) F. Yang, P. Peng, Z.-Y. Yan, H. Fan, X. Li, S. Li, H. Liu, T.-L. Ren, Y. Zhou, Z. L. Wang, D. Wei, *Nat. Energy* **2024**, *9*, 263.

[5] a) D. Wei, F. Yang, Z. Jiang, Z. Wang, *Nat. Commun.* **2022**, *13*, 4965; b) C. Yang, Z. Suo, *Nat. Rev. Mater.* **2018**, *3*, 125.

[6] S. Z. Bisri, S. Shimizu, M. Nakano, Y. Iwasa, *Adv. Mater.* **2017**, *29*, 1607054.

[7] T. Xiong, C. Li, X. He, B. Xie, J. Zong, Y. Jiang, W. Ma, F. Wu, J. Fei, P. Yu, *Science* **2023**, *379*, 156.

[8] Z. Lei, P. Wu, *Matter* **2023**, *6*, 429.

[9] Y. Dobashi, D. Yao, Y. Petel, T. N. Nguyen, M. S. Sarwar, Y. Thabet, C. L. Ng, E. Scabeni Glitz, G. T. M. Nguyen, C. Plesse, *Science* **2022**, *376*, 502.

[10] K. Chen, D. Ho, *Aggregate* **2024**, *5*, e425.

[11] a) Y. Zhang, X. Zhou, N. Zhang, J. Zhu, N. Bai, X. Hou, T. Sun, G. Li, L. Zhao, Y. Chen, L. Wang, C. F. Guo, *Nat. Commun.* **2024**, *15*, 3048; b) Z. Liu, M. Cai, S. Hong, J. Shi, S. Xie, C. Liu, H. Du, J. D. Morin, G. Li, L. Wang, H. Wang, K. Tang, N. X. Fang, C. F. Guo, *Proc. Natl. Acad. Sci. USA* **2024**, *121*, 2320222121; c) Y. Cheng, C. Guo, S. Li, K. Deng, J. Tang, Q. Luo, S. Zhang, Y. Chang, T. Pan, *Adv. Funct. Mater.* **2022**, *32*, 2270274; d) R. Li, Y. Si, Z. Zhu, Y. Guo, Y. Zhang, N. Pan, G. Sun, T. Pan, *Adv. Mater.* **2017**, *29*, 1700253; e) J. Heikenfeld, A. Jajack, J. Rogers, P. Gutruf, L. Tian, T. Pan, R. Li, M. Khine, J. Kim, J. Wang, J. Kim, *Lab Chip* **2018**, *18*, 217.

[12] a) F. Li, X. Cai, G. Liu, H. Xu, W. Chen, *Adv. Funct. Mater.* **2023**, *33*, 2300701; b) L. Jia, L. Li, Z. H. Guo, H. Sun, H. Huang, F. Sun, Z. L. Wang, X. Pu, *Adv. Mater.* **2024**, *36*, 2403830.

[13] W. Zhu, B. Wu, Z. Lei, P. Wu, *Adv. Mater.* **2024**, *36*, 2313127.

[14] S. Wang, T. Yang, D. Zhang, Q. Hua, Y. Zhao, *Adv. Mater.* **2024**, *36*, 2405391.

[15] W. Chen, L. Zhai, S. Zhang, Z. Zhao, Y. Hu, Y. Xiang, H. Liu, Z. Xu, L. Jiang, L. Wen, *Science* **2023**, *382*, 559.

[16] L. Wang, R. Malpass-Evans, M. Carta, N. B. McKeown, F. Marken, *J. Solid State Electrochem.* **2020**, *24*, 2797.

[17] W. Liu, T. Mei, Z. Cao, C. Li, Y. Wu, L. Wang, G. Xu, Y. Chen, Y. Zhou, S. Wang, *Sci. Adv.* **2024**, *10*, eadj7867.

[18] S. J. Yoon, J. T. Park, Y. K. Lee, *Soft Sci.* **2024**, *4*, 30.

[19] P. U. Diehl, G. Zarrella, A. Cassidy, B. U. Pedroni, E. Neftci, presented at 2016 IEEE International Conference on Rebooting Computing (ICRC), IEEE, Piscataway, NJ **2016**, pp. 1.